Fault Estimation for Automotive Electro-Rheological Dampers: LPV-based Observer Approach

Marcelo Menezes Morato, Olivier Sename, Luc Dugard, Manh Quan Nguyen

Fault Estimation for Automotive Electro-Rheological Dampers: LPV-based Observer Approach

Marcelo M. Morato[a,b], Manuel A. Molina Villa[b], Olivier Sename[b], Luc Dugard[b], Manh Quan Nguyen[b]

[a] *Departamento de Automação e Sistemas (*DAS*), Universidade Federal de Santa Catarina, Florianópolis, Brazil, FAX: +55 (48) 3721-9934*
[b] *GIPSA-Lab, Control Systems Department, Grenoble INP, France*

Abstract

This paper presents an LPV method for Fault Estimation, considering Electro-Rheological dampers of automotive suspension systems. Faults upon the dampers are modelled as *Loss of Effectiveness* multiplicative factors, which are estimated with the proposed approach. This framework is based upon an LPV extended-state observer, whose gain is derived from the mixed H_2/H_∞ norm minimization. The method is discussed through simulation and validation tests are realized in a real vehicle test-bench in order to demonstrate the truthfulness and capability of the framework to identify faults on Electro-Rheological dampers.

Keywords: Electro Rheological Damper, Fault Estimation, Polytopic LPV, Suspension Systems, Extended Observer

1. Introduction

Advanced technological processes present evermore an increase on complexity and become more vulnerable to faults due to instrumentation issue. For this, the highlights have been given to Fault Tolerant Control (FTC) schemes, that offer increased process availability by avoiding breakdowns from simple faults, as described by Blanke, Izadi-Zamanabadi, Bogh & Lunau (1997).

Active FTC requires an accurate *online* Fault Detection/Estimation (FD/FE) strategy, so that the control scheme knows real-time information about the state of the controlled plant (faulty or healthy) to compute, if necessary, an adequate reconfiguration mechanism, these concepts can be found in (Zhang & Jiang, 2008; Blanke, Staroswiecki & Wu, 2001; Jiang & Yu, 2012). The book by Mahmoud, Jiang & Zhang (2003) summarizes the most important topics about $FE/FDFTC$.

Email addresses: marcelomnzm@gmail.com (Marcelo M. Morato), mmolina2127@gmail.com (Manuel A. Molina Villa), olivier.sename@gipsa-lab.fr (Olivier Sename), L.Dugard@gipsa-lab.fr (Luc Dugard), quannm.ii@gmail.com (Manh Quan Nguyen)

In terms of the recent development considering *FE* methods, some important references must be remembered. Some nonlinear methodologies have been proposed through literature, as those by: De Persis & Isidori (2001), that propose a geometric approach to detect and isolate faults; Ducard & Geering (2008), that propose a multiple-model adaptive estimation method for unmanned aerial vehicles; Zhang, Jiang & Cocquempot (2009b), that conceive a fast adaptive fault estimation ($FAFE$) method for nonlinear plants; Gao & Ding (2007), that suggest a robust actuator *FE* method for a class of descriptor systems.

Anyhow, a great deal of works suppose linear time-invariance (LTI) system characteristics and resort to parity-space and residual analysis, (Chen & Patton, 2012; Henry & Zolghadri, 2005; Isermann, 1997; Gertler, 1997). The classical *LTI*, model-based *FE* design usually faces problems when dealing with changes upon the observed plant's operational point. Whenever these changes occur, there should not appear (false) fault alarms or the necessity for further observer reconfiguration, which is not always true with these design methods. Still, one key issue that has to be remarked is that most of the mentioned works (both nonlinear and LTI) make use of the redundant availability of sensors in order to conclude about faults. This problem can be overlapped, for instance, with the use of observer-based *FE*, as it has been deeply discussed in (Zhang, Jiang & Shi, 2012).

1.1. Linear Parameter Varying FE *Methods*

From the beginning of the 2000's, the Control Systems Community has worked to overcome these problems, proposing gain-scheduling frameworks to extend the scope of the linear *FE* methods to nonlinear systems. The main idea behind these work is to consider the extension of *LTI* systems to Linear Parameter Varying (LPV) systems in order to model the monitored system. Such models can be used to accurately describe some complex nonlinear plants, see (Mohammadpour & Scherer, 2012).

LPV systems can be understood as a range of systems with known, bounded parametrical variations. An LPV FE scheme, thus, is able to autonomously adjust and schedule observer or detection filter gains. This is a suitable trade-off between full scaled nonlinear designs and *LTI* methods based on a fixed operating condition, since LPV-based *FE* methods provide most of the conveniencies of *LTI* design and still guarantees good performance and stability conditions over a wider operating set.

A few of these works have presented strong results, that also include some experimental validation. These are:

1. The paper by Chen, Patton & Goupil (2016a), that shows application of model-based LPV FE to an industrial benchmark;

2. Also by the same authors, a robust LPV FE is presented in (Chen, Patton & Goupil, 2016b);

3. , An FTC strategy for actuator faults on helicopters is seen in de Oca, Puig, Witczak & Dziekan (2012);

4. An adaptive fault estimation scheme is also applied to helicopter models in Zhang, Jiang & Chen (2009a);

5. Recently, Rotondo, López-Estrada, Nejjari, Ponsart, Theilliol & Puig (2016) proposed fault estimation for discrete LPV systems, with the use of switched observers. Also for discrete-time systems, robust results are found in (Kulcsár & Verhaegen, 2012);

6. LPV FE for descriptor systems has been seen in (López-Estrada, Ponsart, Astorga-Zaragoza & Theilliol, 2013);

7. LPV FE with LFT parameter dependence has been analysed by Wang, Chen & Weng (2014).

1.2. FE *for Automotive Dampers*

This article focuses on the use of LPV-based FE methods, specifically, for the case of actuator faults, considering the application to automotive suspension plants.

In terms of theses vehicle systems, the use of Semi-Active suspensions is ever more present in modern cars. More specifically, the use of Electro-Rheological (ER) Dampers provides continuously variable damping forces, which can enhance driving performances. In terms of modelling and further details on ER dampers, please refer to (Savaresi, Bittanti & Montiglio, 2005; Guo & Zhang, 2012; Do, Sename & Dugard, 2010; Nguyen & Choi, 2009).

While some works have been dedicated to the control of such dampers, the study of faults, failures and monitoring of dampers is quite novel throughout literature, up to the authors' knowledge. Only some few works have dealt with the issue of faulty dampers:

- Moradi & Fekih (2014) proposed a sliding-mode, PID-based, fault tolerant control of vehicle suspensions, considering actuator (damper) faults;

- Fergani, Sename & Dugard (2014b) discussed the issue of re-designing control laws of semi-active suspensions, with LPV/H_∞ design, in the case of damper malfunctions;

- LPV accommodation for damper faults was also studied in (Tudon-Martinez, Varrier, Sename, Morales-Menendez, Martinez & Dugard, 2013; Sename, Tudón-Martínez & Fergani, 2013; Tudón-Martínez, Varrier, Sename, Morales-Menendez, Martinez & Dugard, 2013).

1.3. Contributions Presented

While FE for automotive ER dampers has been studied in (Nguyen, Sename & Dugard, 2015), as far as the authors know, no work has presented experimental validation or applied results of these FE techniques to the vehicle suspension problem. Thus, this is the main motivation of this work. The main contributions, in respect to what has been discussed, are listed below:

(i) Firstly, a novel approach to estimate faults on Electro-Rheological (*ER*) suspension dampers is developed, based on a *Polytopic LPV* Extended-Observer design;

(ii) Then, simulation and experimental validation results are shown, highlighting the accuracy and the success of the proposed technique, that can be implemented in practice with simple micro-controllers, without the need for additional sensors.

The paper is organized as follows: Section 2 introduces Semi-Active suspension systems with Electro-Rheological dampers, depicting dynamic models and introducing the used experimental platform. In section 3, the faulty *ER* damper problem is discussed and the used multiplicative fault representation is detailed. Section 4 presents the proposed *FE* scheme, based on an *LPV* extended-observer. Section 5 gives and discusses some results in terms of simulation and shows the experimental validation. Finally, conclusions are drawn in Section 6.

2. Electro-Rheological Semi-Active Suspension System

2.1. Presentation

In this paper, a Semi-Active vehicle suspension system with four Electro-Rheological dampers is studied. A good trade-off between vehicle's road handling performance and ride confort is strictly related to the vehicle's suspension system. Ever more present in the automotive industry, the Semi-Active suspension systems are to be highlighted, being efficient and at the same time, less energy-consuming and less expensive than purely active suspensions. The use of semi-active suspension systems provides a good balance between costs and performance requirements. This type of suspension is present on new *state-of-the-art top*-cars and a good deal of academic and industrial research is focused on this topic, as seen in (Hrovat, 1997; Tseng & Hrovat, 2015) and others. Further details on semi-active suspension systems are thoroughly discussed in (Patten, He, Kuo, Liu & Sack, 1994; Poussot-Vassal, Spelta, Sename, Savaresi & Dugard, 2012; Fischer & Isermann, 2004; Savaresi, Poussot-Vassal, Spelta, Sename & Dugard, 2010).

2.2. Experimental Platform

This works consideres a real mechatronic test-bench is considered as a tool for validation of the proposed methodology. This testbed is the *INOVE SobenCar*, a $\frac{1}{5}$-scaled vehicle, which allows testing several configurations and use-cases can be tested (refer to full details in (Vivas-Lopez, Alcántara, Nguyen, Fergani, Buche, Sename, Dugard & Morales-Menéndez, 2014; Fergani, Menhour, Sename, Dugard & Novel, 2014a) and on the website (Vivas-Lopez, Alcántara, Nguyen, Fergani, Buche, Sename, Dugard & Morales-Menéndez, 2010)).

This plant, seen in Figure 1, involves four Semi-Active suspension systems using Electro-Rheological dampers that have a force range of $\pm 50\,\mathrm{N}$. Moreover, the user can mimic faulty situations and then, estime faults using an *online FE* scheme on collected data. Figure 2 show the implementation scheme of this system, where a *MATLAB* interpreted controller defines a duty-cycle of a *PWM* signal $d_c(t)$ (given in percentage). This *PWM* signal changes the electric field present inside the *ER* damper's chamber and, consequently, is able to control the fluid's resistance to flow. The *PWM* signals ($d_c(t)$) at 25 kHz vary a controlled voltage inside the range of $[0\,,\,5]$ kV, generated by amplifier modules. The controller can also set reference to road profile generator motors, that mimic various road situations.

Figure 1: *INOVE Soben-Car* Test-Bench

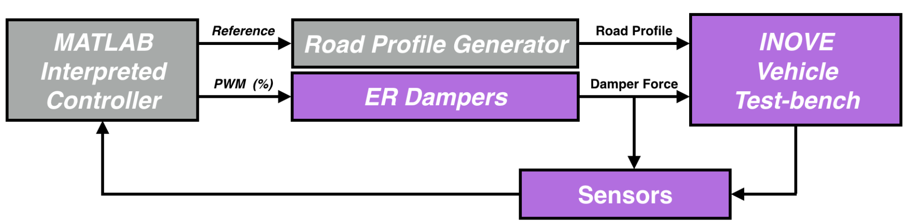

Figure 2: *INOVE Soben-Car* Scheme

2.3. Vehicle Dynamics: Modelling

A semi-active suspension comprises, basically, a spring and a controlled damper. Several modelling approaches can be considered to describe the vertical dynamics of each corner of a vehicle. In this work, a control-oriented *Quarter of a Vehicle* (QoV) model will be used. This model can be used to analyse the behaviour of a single corner of an automotive vehicle independently and does not take into consideration the coupling between the four corners.

A QoV model usually analyses the dynamics of the chassis and the axle of a vehicle, as detailed in Hrovat & Hubbard (1987). These dynamics are the vertical motion of the chassis (given by z_s) and the vertical motion of the axle (given by z_{us}). The suspension system is set between the axle (unsprung mass) and the chassis (sprung mass). The tire is, simply, represented by a linear spring, with k_t coefficient. As detailed in (Sammier, Sename & Dugard, 2003), the damping coefficient of the tire is small and may be omitted for control purposes. In terms of notation, k_s represents the suspensions spring coefficient, m_s and m_{us} the sprung and unsprung masses, respectively, z_r the road profile, z_s and z_{us} the relative displacements of the sprung and unsprung masses, respectively. The suspension system's deflection is given by $z_{def}(t) = z_s(t) - z_{us}(t)$.

Applying and linearizing the equations of motion of the QoV model with a semi-active suspension around a steady-state operation point, one arrives at the following dynamical equations, as describes Fischer & Isermann (2004):

$$\begin{aligned} m_s \ddot{z}_s(t) &= -k_s z_{def}(t) + F_{ER}(t) \\ m_{us} \ddot{z}_{us}(t) &= k_s z_{def}(t) - F_{ER}(t) - k_t(z_{us}(t) - z_r(t)) \end{aligned} \tag{1}$$

where $F_{ER}(t)$ represents the force of an Electro-Rheological controlled damper.

Now, this work uses a *state-space* representation of this semi-active suspension of a QoV model with a *ER* damper that is subject to faults, by using equation (1) and by considering system states $(x(t))$, disturbance input $(w(t))$ and measured outputs $(y(t))$, respectively, as:

$$x(t) = \begin{bmatrix} z_s(t) & \dot{z}_s(t) & z_{us}(t) & \dot{z}_{us}(t) \end{bmatrix}^T \tag{2}$$

$$w(t) = \begin{bmatrix} z_r(t) \end{bmatrix}^T \tag{3}$$

$$y(t) = \begin{bmatrix} z_{def}(t) & \ddot{z}_s(t) \end{bmatrix}^T \tag{4}$$

Remark 1. This used measurements are, in a certain way, common on vehicular suspension systems. The suspension deflection $(z_{def}(t))$ measurement can be acquired with the use of relative displacement sensors and the sprung mass acceleration $(\ddot{z}_s(t))$ arises from the use of accelerometers.

Finally, it is taken into account that the control input $u(t)$ is the damper force that acts upon the vehicle system, this is $u(t) = F_{ER}(t)$. Then, one is lead to:

$$\begin{aligned} \dot{x}(t) &= \mathbf{A}x(t) + \mathbf{B}_1 w(t) + \mathbf{B}_2 u(t) \\ y(t) &= \mathbf{C}x(t) + \underbrace{\mathbf{D}_1}_{=\vec{0}} w(t) + \mathbf{D}_2 u(t) \end{aligned} \tag{5}$$

where the matrices in (5) are all constant and defined in equations (6) to (9).

$$\mathbf{A} = \begin{bmatrix} 0 & 1 & 0 & 0 \\ \frac{-k_s}{m_s} & 0 & \frac{k}{m_s} & 0 \\ 0 & 0 & 0 & 1 \\ \frac{k_s}{m_{us}} & 0 & -\frac{(k_t+k_s)}{m_{us}} & 0 \end{bmatrix} \tag{6}$$

$$\mathbf{B}_1 = \begin{bmatrix} 0 \\ 0 \\ 0 \\ \frac{k_t}{m_{us}} \end{bmatrix} \quad \mathbf{B}_2 = \begin{bmatrix} 0 \\ -\frac{1}{m_s} \\ 0 \\ \frac{1}{m_{us}} \end{bmatrix} \tag{7}$$

$$\mathbf{C} = \begin{bmatrix} 1 & 0 & -1 & 0 \\ \frac{-k_s}{m_s} & 0 & \frac{k_s}{m_s} & 0 \end{bmatrix} \tag{8}$$

$$\mathbf{D}_2 = \begin{bmatrix} 0 \\ \frac{1}{m_s} \end{bmatrix} \tag{9}$$

The parameter identification of the masses (axle and chassis), spring coefficient, tire (spring) coefficient and nominal damping coefficient of the used experimental plateform has previously been done in (Vivas-Lopez, Alcántara, Nguyen, Fergani, Buche, Sename, Dugard & Morales-Menéndez, 2014). In Table 1, the numerical values for each of the parameters of this vehicle testbed are given, considering only a single-corner of this vehicle (front-right corner).

Table 1: Vehicle Model Parameters: *INOVE Soben-car*

Parameter	Value	Unit
m_s	2.27	kg
m_{us}	0.25	kg
k_t	12269.81	N/m
k_s	1396.80	N/m

Remark 2. The validation of the *Quarter-of-Vehicle* model is discussed in (Savaresi, Poussot-Vassal, Spelta, Sename & Dugard, 2010) in terms of frequency and time-domain results. Therein, it can be seen that this model can accurately represent the vertical dynamics of a corner of a vehicle.

Assumption 1. In the sequel, it is assumed that some model of the road profile disturbance is known. This can be expressed mathematically by:

$$w(t) = \overbrace{w_{\mathrm{m}}(t)}^{\text{known model}} + \overbrace{\delta w(t)}^{\text{unknown}} \tag{10}$$

$$\dot{w_{\mathrm{m}}}(t) = \mathbf{A}_{mw} w_{\mathrm{m}}(t) + \overbrace{\nu(t)}^{\text{noise}} \tag{11}$$

Such kind of description allows to consider several types of road profiles. It is worth noting that, according to the considered type, the dimension of $w_m(t)$ may change.

The above Assumption is not so absurd. Modern cars present cameras and other features than surve to this purpose. This information on the type of road profile ($\mathbf{A}_{mw}$) may also come from an external adaptive road profile estimator, as proposed in (Tudón-Martínez, Fergani, Sename, Martinez, Morales-Menendez & Dugard, 2015). Another efficient option to compute the disturbance model is to consider a frequency-wise approach, as proposed by Unger, Schimmack, Lohmann & Schwarz (2013). What is referred here as $\mathbf{A}_{mw}$ can be understood as the *ISO* road surface categories (ISO 8608:2016).

2.4. The Electro-Rheological Damper

This work is mainly concerned by the study of Electro-Rheological dampers. Considering the use of *ER* dampers, one may vary the amount of damping by exploiting the physical property of the fluid that flows inside the shock-absorber's chamber. *ER* fluids can be understood as a mixture of oil and micron-sized particles which are sensitive to an electrical field.

In the experimental testbed, a PWM signal changes the electric field present inside the *ER* damper's chamber and, consequently, is able to control the fluid's resistance to flow and, thus, the force delivered by the damper, represented herein by $F_{ER}(t)$.

When there is no electric field applied to the damper chamber, the *ER* fluid is almost free to flow and the damper force is considered as purely passive. On the other hand, when an electric field is applied, the particles of the *ER* fluid act as dipoles and form chains. This implies that the flow of the fluid becomes similar to a *visco-plastic* and the damping coefficient increases. Synthetically, stronger the electric field present, greater the damping coefficient.

2.5. ER *Damper Force: Modelling*

In this work, the *ER* damper force is modelled considering a parametric analytical model adapted from (Guo, Yang & Pan, 2006), which has already expressed good results.

As shown below, in equations (12)-(16), this force is divided into controlled and passive parts:

$$\begin{aligned}
\tau\frac{dF_{ER}}{dt}(t)+F_{ER}(t) &= F_{ER}^{\text{Static}}(t) && (12)\\
\text{with} & \\
F_{ER}^{\text{Static}}(t) &= \overbrace{F_{ER}^{\text{Spring}}(t)+F_{ER}^{\text{Purely Passive}}(t)}^{\text{passive}} && (13)\\
&+ \underbrace{F_{ER}^{\text{Controlled}}(t)\text{sign}\{\dot{z}_{def}(t)\}}_{\text{controlled}} & \\
F_{ER}^{\text{Spring}}(t) &\approx k_{nom}z_{def}(t) && (14)\\
F_{ER}^{\text{Purely Passive}}(t) &= c_{nom}\dot{z}_{def}(t) && (15)\\
F_{ER}^{\text{Controlled}}(t) &= \beta_1 d_c(t)^{\beta_2} && (16)
\end{aligned}$$

In these equations: τ is the dynamical time constant of the *ER* damper model; β_1 and β_2 are intrinsic parameters of the *ER* fluid, linked to the yield stress; k_{nom} and c_{nom} are constant parameters.

Analyzing equations (12)-(16), one observes that the damper force has a first-order dynamical behaviour and depends on three distinctive characteristics: the purely passive damper force, always present, due to the *ER* fluid flow, named $F_{ER}^{\text{Purely Passive}}(t)$ and given by equation (15); the spring-like behaviour of the damper, named $F_{ER}^{\text{Spring}}(t)$; and the controlled force, due to the presence of the electric field, given by $F_{ER}^{\text{Controlled}}(t)$ in equation (16).

2.6. Parameter Identification

Considering the presented Electro-Rheological damper force modelling, some parameter identification tests were performed. Experiments were conducted on the testbed, using the measurements of the variation of the damper force to different road profiles with the *Nonlinear Least Squares* method. The estimated values of k_{nom}, c_{nom}, β_1 and β_2 are presented in Table 2. The dynamical time constant was fixed by empirical testing.

Table 2: Other *ER* Damper Parameters

Parameter	Value	Unit
k_{nom}	47.2458	N/m
c_{nom}	59.97	N.s/m^2
τ	20	ms
β_1	35.8	–
β_2	1	–

2.7. Validation Results

Some validation results are presented, considering this detailed Electro-Rheological damper, that demonstrate the accuracy of the model.

Considering the scaled-vehicle experimental test-bench described in Section 2.2, an experiment was done with the road profile $w(t)$ of sequential 10 mm bumps. The PWM signal, $d_c(t)$, for this validation, was fixed at 10 %.

Figure 3 shows the comparison between the actual damper force (measured in N by a force sensor present in this testbed) and the expected damper force computed with the ER damper model (12)-(16). It presents an overall good estimation of the ER damper force, given the accurate knowledge of the PWM signal ($d_c(t)$), the suspension deflection ($z_{def}(t)$) and the deflection velocity ($\dot{z}_{def}(t)$). Note that $\dot{z}_{def}(t)$ is computed numerically, with the use of derivative filtering, as the average bandwidth of $z_{def}(t)$ is known.

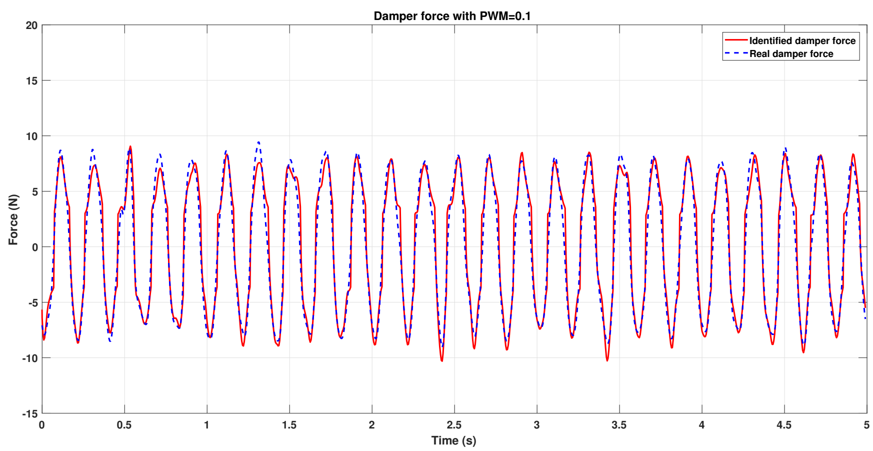

Figure 3: Electro Rheological Damper Force: Model *vs.* Real Data

3. The Faulty *ER* Damper Situation

An Electro-Rheological damper can fail due to, basically, three kinds of faults: oil leakage, physical deformation or presence of air inside the ER fluid, the first being the most common.

3.1. Modelling

If the amount of damping fluid decreases, due to leakage, the flow inside the ER damper chamber consequently decreases, which implies a loss of the effectiveness of the damper's force. It is assumed that only a portion of oil leaks from the damper chamber, not all oil. A complete leak would lead to a total failure, which is not the main interest here. Partial faults are much harder to detect.

Firstly, it is assumed that the ER damper force $F_{ER}(t)$, the control input (actuation) to the vehicle's suspension system, is subject to a multiplicative fault.

This multiplicative factor is considered as a **Loss of Effectiveness Fault**. This multiplicative fault representation has been firstly presented in (Sename, Tudón-Martínez & Fergani, 2013) and (Tudón-Martínez, Varrier, Sename, Morales-Menendez, Martinez & Dugard, 2013) and later used in (Hernández-Alcántara, Tudón-Martínez, Amézquita-Brooks, Vivas-López & Morales-Menéndez, 2016), which introduced a solid framework for the modelling of faults.

Generally speaking, the real actuation upon the suspension system, given by $u_f(t)$, depends proportionally to the damper force $u(t) = F_{ER}(t)$. Thus, whenever there is a fault in an *ER* damper, the suspension system's representation, given by equation (5), should be re-written as:

$$\begin{array}{rclllll} \dot{x}(t) & = & \mathbf{A}x(t) & + & \mathbf{B}_1 w(t) & + & \mathbf{B}_2 u_f(t) \\ y(t) & = & \mathbf{C}x(t) & + & \mathbf{D}_1 w(t) & + & \mathbf{D}_2 u_f(t) \end{array} \tag{17}$$

The faulty control input $u_f(t)$ should then be taken as:

$$u_f(t) = \underbrace{\alpha}_{\text{Fault!}} \times F_{ER}(t) \tag{18}$$

Remark 3. Once again, $F_{ER}(t)$ represents the damper force in a faultless scenario. In this case, one has $\alpha = 1$ and, in the worst scenario (where the damper completely fails and is rigid), one has $\alpha = 0$. So, $\alpha(t) \in [0\,,\,1]$. As $\alpha(t)$ is a time-function, it can be used to represent any kind of faulty situation.

As stated by Nguyen, Sename & Dugard (2015), it is worth noting also that even if $\alpha(t)$ is assumed to be constant, the corresponding additive fault magnitude on the faulty damper is given by $f(t) = (\alpha - 1)F_{ER}(t)$, which is a time varying signal that depends on the value of the expected damper force $F_{ER}(t)$. Thanks to the multiplicative representation, the information on the actuator fault $\alpha(t)$ is considered as constant or slow-varying and, thus, it is assumed that $\dot{\alpha}(t) = 0$.

3.2. Experimental Simulation of the Faulty Damper

In order to illustrate the effect of an oil leakage, the *INOVE Soben-Car* experimental platform is used to mimic the effects of a faulty situation. For this, the *PWM* signal $d_c(t)$ is taken as a function of the desired mimicked faulty (or fault-free) *PWM* input $(\overline{d_c}(t))$:

$$d_c(t) = \mathcal{F}(\overline{d_c}(t), \alpha^{\text{desired}}(t)) \tag{19}$$

The function $\mathcal{F}(\cdot)$ is taken as the inverse of the damper force model depicted in Section 2.5. As a result, the actual force provided by the *ER* damper is given by $u_f(t) = \alpha^{\text{desired}}(t) \times F_{ER}(t)$. Figure 4 shows how a fault can be mimicked in the experimental test-bench. Such an experimental simulation of a fault is coherent with the work presented by Hernández-Alcántara, Tudón-Martínez, Amézquita-Brooks, Vivas-López & Morales-Menéndez (2016).

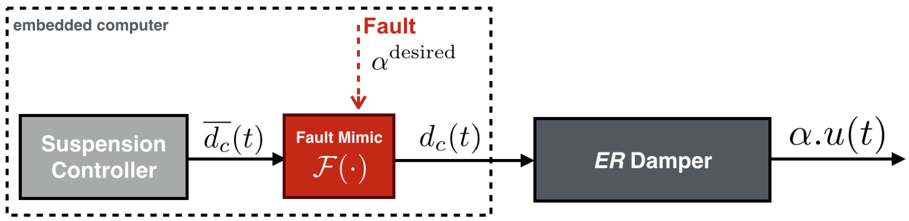

Figure 4: Experimental Fault Mimic

4. Proposed Fault Estimation Scheme

The main goal of this Section is to answer the question highlighted by this work: how can these (already modelled) damper faults be identified and diagnosed ?

This Section firstly presents a *polytopic* state-space representation of the studied automotive suspension, then an extended observer is designed and the proposed *FE* solution is thoroughly developed.

4.1. Polytopic LPV *Representation*

Firstly, as of Assumption 1, some model on the type of road disturbance is known. This has been described by equations (10)-(11).

Assumption 2. It is also assumed that the measured outputs $y(t)$ are also subject to some additive noise $\nu(t)$. This is typical in any real instrumented; so, one has:

$$y(t) \quad = \quad \mathbf{C}x(t) + \mathbf{D}_1 w(t) + \mathbf{D}_2 u_f(t) + \mathbf{D}_\nu \nu(t) \tag{20}$$

where $\mathbf{D}_\nu$ is a noise distribution matrix.

Assumption 3. Last but not least, it is also assumed (and reaffirmed) that the fault factor $\alpha(t)$ is slow-varying, with $\dot{\alpha}(t) \approx 0$.

From this point, then, Equations (18), (10), (11) and (20) are coupled together with Equation (17) and the following extended state-space representation of the studied system is obtained:

$$
\begin{aligned}
\overbrace{\begin{bmatrix} \dot{x}(t) \\ \dot{\alpha}(t) \\ \dot{w_m}(t) \end{bmatrix}}^{\dot{x_a}(t)} &= \overbrace{\begin{bmatrix} \mathbf{A} & \underbrace{\mathbf{B}_2 F_{ER}(t)}_{\mathbf{B}_\alpha} & \mathbf{B}_1 \\ 0 & 0 & 0 \\ 0 & 0 & \mathbf{A}_{mw} \end{bmatrix}}^{A}_{a} \overbrace{\begin{bmatrix} x(t) \\ \alpha(t) \\ w_m(t) \end{bmatrix}}^{x_a(t)} \\
&+ \overbrace{\begin{bmatrix} \mathbf{B}_1 \\ 0 \\ 0 \end{bmatrix}}^{\mathbf{B}_w} \delta w(t) + \overbrace{\begin{bmatrix} 0 \\ 0 \\ \mathbb{I} \end{bmatrix}}^{\mathbf{B}_\nu} \nu(t) \qquad (21) \\
y(t) &= \underbrace{\begin{bmatrix} \mathbf{C} & \overbrace{\mathbf{D}_2 F_{ER}}^{\mathbf{D}_\alpha} & \mathbf{D}_1 \end{bmatrix}}_{\mathbf{C}_a} x_a(t) \\
&+ \mathbf{D}_1 \delta w(t) + \mathbf{D}_\nu \nu(t)
\end{aligned}
$$

It is important to notice that the matrices $\mathbf{A}_a$ and $\mathbf{C}_a$ are affine on $F_{ER}(t)$, due (respectively) to the terms $\mathbf{B}_\alpha$ and $\mathbf{D}_\alpha$.

Assuming that the desired damper force signal $F_{ER}(t)$ is a **known** variable, computed with the *ER* damper force model (12)-(16), and **bounded**, due to physical saturation constraints of the platform's semi-active dampers, an *LPV* approach can be used to represent this system (21). This is:

$$F_{ER}(t) \in \mathcal{U}_{\text{sat}} = \{u_{min} = -21\,\mathrm{N} \leq \mathrm{F_{ER}(t)} \leq 21\,\mathrm{N} = \mathrm{u_{max}}\} \tag{22}$$

Thus, this study considers $F_{ER}(t)$ as a scheduling parameter ρ, which satisfies:

$$0 < \rho_{min} \leq \rho \leq \rho_{max} \tag{23}$$

Then, taking $\rho = F_{ER}(t)$, the matrices $\mathbf{B}_\alpha$ and $\mathbf{D}_\alpha$ can be re-written, respectively, as $\mathbf{B}_\alpha = \mathbf{B}_2\rho$ and $\mathbf{D}_\alpha = \mathbf{D}_2\rho$. From this point, matrices $\mathbf{A}_a$ and $\mathbf{C}_a$ become affine in ρ and the augmented system (21) is *LPV*.

A *polytopic LPV* representation of (21) is presented below, considering a polytope $\mathcal{P}$ defined by ρ at its vertices $\rho = \rho_{min}$ and $\rho = \rho_{max}$.

$$\sum_{k=1}^{2} \beta_k(\rho) \left[\begin{array}{c|c|c} \mathbf{A}_a^k & \mathbf{B}_w & \mathbf{B}_\nu \\ \hline \mathbf{C}_a^k & \mathbf{D}_1 & \mathbf{D}_\nu \end{array}\right] \tag{24}$$

with

$$\sum_{k=1}^{2} \beta_k(\rho) = 1 \ , \ \ \beta_k(\rho) > 0 \tag{25}$$

where each system $\left[\begin{array}{c|c|c} \mathbf{A}_a^k & \mathbf{B}_w & \mathbf{B}_\nu \\ \hline \mathbf{C}_a^k & \mathbf{D}_1 & \mathbf{D}_\nu \end{array}\right]$ is an individual *LTI* system *frozen* at the vertex k of the polytope $\mathcal{P}$ defined by the boundaries of $\mathcal{U}_{\text{sat}}$.

4.2. Extended Observer

As the faulty system is represented through an augmented framework with states $x_a(t)$, the estimation of $\alpha(t)$ can be achieved with an accurate tracking of these augmented states.

Synthetically: the problem is to identify the fault term $\alpha(t)$ only through the available measurements of $y(t)$. This is done here by an observer-based approach. Figure 5 represents the complete fault detection and diagnosis problem proposed in this paper, considering the real test-bench. In this Figure, the "*ER Damper Model*" block stands for the model given by equations (12)-(16).

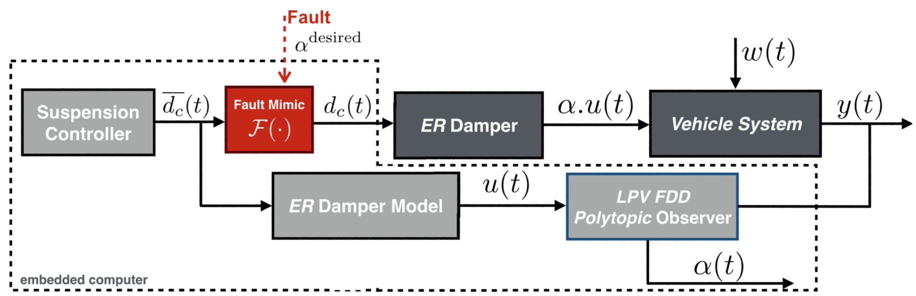

Figure 5: Complete *FE* Problem: *ER* Damper Faults

As seen in (Rodrigues, Hamdi, Theilliol, Mechmeche & BenHadj Braiek, 2015; Grenaille, Henry & Zolghadri, 2008), a polytopic *LPV* observer to asymptotically track the states $x_a(t)$ can be defined as follows:

$$\begin{aligned} \dot{\hat{x}}_a(t) &= \mathbf{A}_a(\rho)\hat{x}_a(t) + \mathbf{L}(\rho).[y(t) - \mathbf{C}_a(\rho)\hat{x_a}(t)] \\ \hat{\alpha}(t) &= \underbrace{\begin{bmatrix} 0_{\text{size}(x)} & \mathbb{I}_{\text{size}(\alpha)} & 0_{\text{size}(w)} \end{bmatrix}}_{\mathbf{E}} \hat{x_a}(t) \end{aligned} \tag{26}$$

where $\hat{x}_a(t)$ and $\hat{\alpha}(t)$ stand, respectively, for the estimation of the augmented states and the loss of effectiveness fault term.

The dynamics of the estimation error ($e(t) = x_a(t) - \hat{x}_a(t)$) and fault estimation error ($e_\alpha(t) = \alpha(t) - \hat{\alpha}(t)$) are given by:

$$\begin{aligned} \dot{e}(t) &= [\mathbf{A}_a(\rho) - \mathbf{L}(\rho)\mathbf{C}_a(\rho)]e(t) \\ &\quad + (\mathbf{B}_w - \mathbf{L}(\rho)\mathbf{D}_1)\delta w(t) \\ &\quad + (\mathbf{B}_\nu - \mathbf{L}(\rho)\mathbf{D}_\nu)\nu(t) \end{aligned} \tag{27}$$

$$e_\alpha = \mathbf{E}e(t) \tag{28}$$

Given the polytopic representation used throughout this work, the system (27)-(28) can be also expressed as:

$$\sum_{k=1}^{2} \beta_e k(\rho) \left[\begin{array}{c|c|c} (\mathbf{A}_a^k - \mathbf{L}^k \mathbf{C}_a^k) & (\mathbf{B}_w - \mathbf{L}^k \mathbf{D}_1) & (\mathbf{B}_\nu - \mathbf{L}^k \mathbf{D}_\nu) \\ \hline \mathbf{E} & 0 & 0 \end{array} \right] \tag{29}$$

with

$$\sum_{k=1}^{2} \beta_e^k(\rho) = 1 \ , \ \ \beta_e k(\rho) > 0 \tag{30}$$

where each system $\left[\begin{array}{c|c|c} (\mathbf{A}_a^k - \mathbf{L}^k \mathbf{C}_a^k) & (\mathbf{B}_w - \mathbf{L}^k \mathbf{D}_1) & (\mathbf{B}_\nu - \mathbf{L}^k \mathbf{D}_\nu) \\ \hline \mathbf{E} & 0 & 0 \end{array} \right]$ is an individual *LTI* system, *frozen* at the vertex k of the polytope $\mathcal{P}$ defined by the boundaries of $\mathcal{U}_{\text{sat}}$.

Remark 4. Note that, as this work opts for a (decoupled) *QoV* model, four separate *FE* observers on the form (26) can be designed, individually, for each corner of the vehicle. This provides simplicity and a straightforward implementation that could be done on simple microcontrollers embedded to each *ER* damper, as it deals with sum of two simple linear models and there is no need for optimization procedure.

A full vehicle model could have been considered, but this would only enlarge the computational burden without actually leading to better results, given that the effect of the damper faults can be entirely felt by the *QoV* model.

4.3. Specific Problem

As seen in equation (27), the stability of the estimation error depends on the gain matrix $L(\rho)$. So, the following specific problem is traced, adapted from (Karimi, 2008; Scherer, Gahinet & Chilali, 1997; Khosrowjerdi, Nikoukhah & Safari-Shad, 2004).

Problem 1. *The mixed H_2/H_∞* LPV *observer problem is defined as follows: Find a gain matrix $L(\rho)$, affine in the scheduling parameter ρ and defined within the polytope $\mathcal{P}$ so that the fault estimation error dynamics, given by system (27)-(28), are exponentially stable when $\nu(t)$ and $\delta w(t)$ are null, and, such that the two following objective functions are minimized:*

$$J_{H_2} \ = \ ||\tfrac{e_\alpha}{\nu}||_2 \leq \gamma_{H_2} \quad \textit{under} \quad e(t)|_{t=0} = 0 \quad \textit{and} \quad \delta w(t) \equiv 0 \tag{31}$$

$$J_{H_\infty} \ = \ ||\tfrac{e_\alpha}{\delta w}||_\infty \leq \gamma_{H_\infty} \quad \textit{under} \quad e(t)|_{t=0} = 0 \quad \textit{and} \quad \nu(t) \equiv 0 \tag{32}$$

Notice that this H_2/H_∞ criterion is a suitable choice in order to compute the matrix gain $L(\rho)$ of the proposed extended observer and to guarantee the stability of (27), as it represents a noise filtering, disturbance attenuation framework and, specifically, for the following reasons:

- The H_2 norm of a system, from a stochastic point-of-view, is equal to the square root of the asymptotic variance of the output when the input is a white noise, which means that the measurement noise effect will be diminished when estimating the loss of effectiveness fault term $\alpha(t)$ (*impulse-to-energy* gain minimization), taking the measurement noise as the input to the fault estimation error system (27)-(28);

- The H_∞ norm of a system is understood as the induced *energy-to-energy* gain, being the worst case attenuation level of a system to a given input, which means that the influence of the additive disturbance uncertainty $\delta w(t)$ on the estimation of α will be minimized, taking $\delta w(t)$ as the input to the fault estimation error system (27)-(28). Mathematically, the H_∞ norm definition of the error system (taking $\delta w(t)$ as input) is given below:

$$||T_{e_\alpha \delta w}||_\infty \quad = \quad \sup_{\delta w \in \mathcal{H}_2} \frac{||e_\alpha||_2}{||\delta w||_2} \tag{33}$$

4.4. Problem Solution

In this article, the solution to this polytopic LPV observer with a H_2/H_∞ criterion is given by the following lemma. This solution provides the FE scheme to be applied to ER dampers.

Lemma 1. *Considering the system (21) and observer (26). Problem 1 is solved if, given β, there exist positive definite matrices $\boldsymbol{P}$ and $\boldsymbol{N}$ and a rectangular matrix $\boldsymbol{Q}(\rho)$, affine in ρ, such that the following* LMI*s are satisfied for all $\rho \in \mathcal{P}$. The maximal variance of the estimation error, due to the presence of measurement noise $\nu(t)$ is given by $Trace(\boldsymbol{N}) = \gamma_{H_2}$ and the maximal amplification of the estimation error due to the presence of the uncertain disturbance $\delta w(t)$ is given by γ_{H_∞}. The scalar β is an exponential stability decay-rate condition imposed on the eigenvalues of $(\boldsymbol{A}_a(\rho) - \boldsymbol{L}(\rho)\boldsymbol{C}_a(\rho))$: these must be greater, in module, than β, inside region $\mathcal{R}_p$ of complex plane $\mathbb{C}$.*

$$Trace(\boldsymbol{N}) \quad \leq \quad \gamma_{H_2} \tag{34}$$

$$\begin{bmatrix} \mathcal{M}_{11}^1 & \mathcal{M}_{12}^1 \\ \star & \mathcal{M}_{22}^1 \end{bmatrix} \quad < \quad 0 \tag{35}$$

$$\mathcal{M}^2 \quad < \quad 0 \tag{36}$$

$$\begin{bmatrix} \mathcal{M}_{11}^3 & \mathcal{M}_{12}^3 \\ \star & \mathcal{M}_{22}^3 \end{bmatrix} \quad > \quad 0 \tag{37}$$

$$\begin{bmatrix} \mathcal{M}_{11}^4 & \mathcal{M}_{12}^4 & \mathcal{M}_{13}^4 \\ \star & -\mathbb{I}\gamma_{H_\infty} & 0 \\ \star & \star & -\mathbb{I}\gamma_{H_\infty} \end{bmatrix} \quad < \quad 0 \tag{38}$$

$$
\begin{aligned}
\mathcal{M}^1_{11} &= \boldsymbol{A}^T_a(\rho)\boldsymbol{P} + \boldsymbol{P}\boldsymbol{A}_a(\rho) && (39)\\
&- \boldsymbol{C}^T_a(\rho)\boldsymbol{Q}^T(\rho) - \boldsymbol{Q}(\rho)\boldsymbol{C}_a(\rho)\\
\mathcal{M}^1_{12} &= -\boldsymbol{Q}(\rho) && (40)\\
\mathcal{M}^1_{22} &= -(\boldsymbol{E}^T\boldsymbol{E}) && (41)\\
\mathcal{M}^2 &= 2\beta\boldsymbol{P} + \boldsymbol{A}^T_a(\rho)\boldsymbol{P} + \boldsymbol{P}\boldsymbol{A}_a(\rho) && (42)\\
&- \boldsymbol{C}^T_a(\rho)\boldsymbol{Q}^T(\rho) - \boldsymbol{Q}(\rho)\boldsymbol{C}_a(\rho)\\
\mathcal{M}^3_{11} &= \boldsymbol{N} && (43)\\
\mathcal{M}^3_{12} &= \boldsymbol{B}^T_\nu\boldsymbol{P}^T(\rho) - \boldsymbol{D}^T_\nu\boldsymbol{Q}^T(\rho) && (44)\\
\mathcal{M}^3_{22} &= \boldsymbol{P} && (45)\\
\mathcal{M}^4_{11} &= \boldsymbol{A}^T_a(\rho)\boldsymbol{P}^T(\rho) + \boldsymbol{P}\boldsymbol{A}_a(\rho) && (46)\\
&- \boldsymbol{C}^T_a(\rho)\boldsymbol{Q}^T(\rho) - \boldsymbol{Q}(\rho)\boldsymbol{C}_a(\rho)\\
\mathcal{M}^4_{12} &= \boldsymbol{P}\boldsymbol{B}_w - \boldsymbol{Q}(\rho)\boldsymbol{D}_1 && (47)\\
\mathcal{M}^4_{13} &= diag\{\boldsymbol{E}\} && (48)
\end{aligned}
$$

Therefore, the observer gain matrix $\boldsymbol{L}(\rho)$ *is taken as* $\boldsymbol{L}(\rho) = \boldsymbol{P}^{-1}\boldsymbol{Q}(\rho)$.

Proof. Proof is straightforward and immediate from what is presented in Khosrowjerdi, Nikoukhah & Safari-Shad (2004) □

Remark 5. The following remarks are relevant for the proposed Lemma:

1. This is a non-convex problem. In order to solve it, γ_{H_∞} is fixed, whereas γ_{H_2} is minimized. This is detailed in (Poussot-Vassal, 2008). If a trade-off between H_2 and H_∞ performances is sought, an adequate approach would be to solve the *LMI*s minimizing the convex sum $\mathcal{S}(\gamma_{H_2}, \gamma_{H_\infty}) = \theta\gamma_{H_2} + (1-\theta)\gamma_{H_\infty}$ with $\theta \in [0\,,1]$, as detailed in Yamamoto, Koenig, Sename & Moulaire (2015). This compromise, well known in economy, game theory and engineering, is also called the Pareto optimality. For more details on this matter, the reader is invited to refer to (Pardalos, Migdalas & Pitsoulis, 2008);

2. This approach can be easily modified to set the H_2 and H_∞ conditions to all estimated states, taking $\mathbf{E} = \mathbb{I}$;

3. A weighting function can be appropriately introduced to specify the frequency range in which sensor noises should be attenuated. Besides, (obviously) sensor noise is considered as a high frequency signal.

The interest of this polytopic LPV approach is that the *LMI*s (34)-(37) are computed *offline*, considering each vertex of the polytope $\mathcal{P}$ with the same mixed H_2/H_∞ criterion. As there is only one scheduling parameter $\rho = F_{ER}(t)$, this work is concerned only in solving the given LMI problem at $\rho = u_{max}$, finding $\mathbf{L}_{max}$, and at $\rho = u_{min}$, finding $\mathbf{L}_{min}$.

Finally, the gain matrix $\mathbf{L}(\rho)$ given by equation (49), is affine in the scheduling parameter ρ and guarantees the exponential stability of the estimation error dynamics of the proposed LPV observer. This means that, in finite time, the fault terms will be accurately determined and $\hat{\alpha} \to \alpha$.

$$\begin{aligned} \mathbf{L}(\rho) \quad = \quad & \left(\frac{\rho_{max} - \rho}{\rho_{max} - \rho_{min}}\right) .\mathbf{L}_{min} + \\ & \left(\frac{\rho - \rho_{min}}{\rho_{max} - \rho_{min}}\right) \mathbf{L}_{max} \end{aligned} \tag{49}$$

4.5. Frequency-Domain Analysis

Given the solution of the LMI problem (34)-(38) in Lemma 1, let some frequency-domain analysis of the estimation error dynamics, $e(t)$, be presented.

In Table 3, the achieved values for γ_{H_2} and γ_{H_∞} are presented, considering the use of the following softwares: *MATLAB* (Mathworks, 2017), *Yalmip* (Lofberg, 2004) and *SDP*3 (Toh, Todd & Tütüncü, 1999).

Table 3: *LMI* Solutions

γ_{H_2}	0.0659
γ_{H_∞}	0.2532

Disturbance Effect

In Figure 6, a frequency Bode plot for $e_\alpha(t)$ is given, taking $\delta w(t)$ as an input, **frozen** at different regions of the polytope $\mathcal{P}$, considering:

$$\rho \quad = \quad \{\rho_{min}\,, -10\,, 0\,, 10\,, \rho_{max}\} \tag{50}$$

The solution presents good results in terms of disturbance attenuation, as the upper H_∞ bound is quite sufficient (around $-12\,\text{dB}$) considering that the order of magnitude of $\delta w(t)$ is of some millimeters.

Noise Effect

In Figure 7, a frequency Bode plot for $e_\alpha(t)$ is seen, taking $\nu(t)$ as an input, **frozen** at different regions of the polytope given by Equation (50). The solution presents good results in terms of noise rejection, taking in consideration that $\nu(t)$ represents instrumentation noise, which is intrinsically of high frequencies, wherein the upper bound on the singular values rapidly decreases (low-pass filter behaviour).

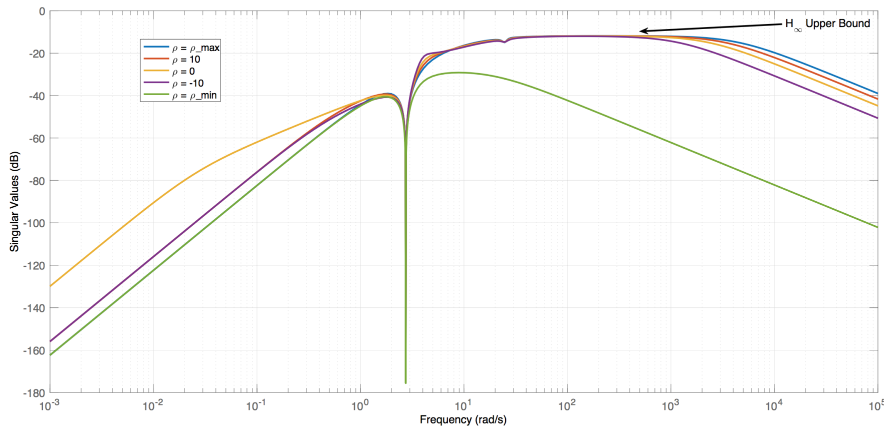

Figure 6: Estimation Error Frequency Plot - H_∞ Bounds on Disturbance

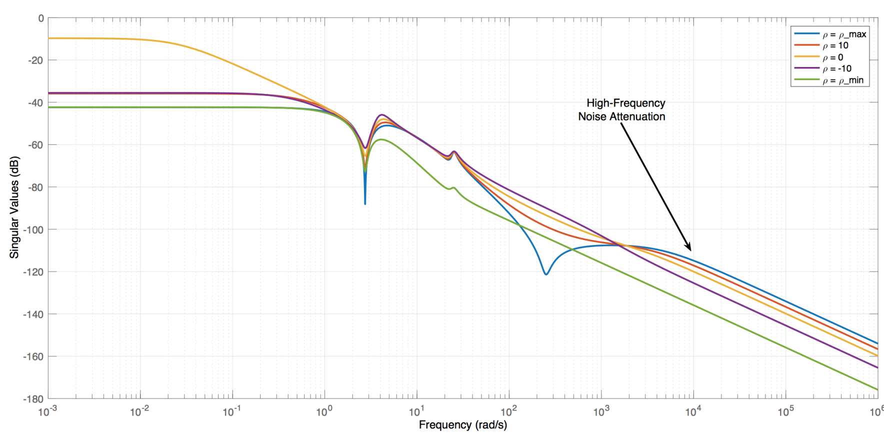

Figure 7: Estimation Error Frequency Plot - H_2 Bounds on Noise

5. Results: Simulation and Experimental Validation

In this Section, validation results are presented, considering the problem of estimating and identifying faults on a semi-active *ER* dampers.

5.1. Simulation Results

In order to provide truthful, realistic tests, the following simulation results consider a full nonlinear vehicle model, as described in (Poussot-Vassal, Sename, Dugard, Gaspar, Szabo & Bokor, 2011; Fergani, Menhour, Sename, Dugard & D'Andréa-Novel, 2016). This model includes nonlinear suspension forces and has been validated with a real car. In order to mimic measurement noise, a high-frequency signal ($\nu(t)$) is added to each component of $y(t)$.

A sinusoidal road profile disturbance $w(t)$, that could represent a series of bumps for a vehicle running on a dry road at constant speed, is used (Doumiati, Martinez, Sename, Dugard & Lechner, 2017). Also the *PWM* control signal $d_c(t)$, responsible for changing the damping force, is taken as a series of steps to imitate some control law issued to guarantee vehicle performances. The suspension *ER* damper is initially fault-less ($\alpha(0) = 1$). This described scenario is summarized in Figure 8, where $d_c(t)$ and $w(t)$ are given.

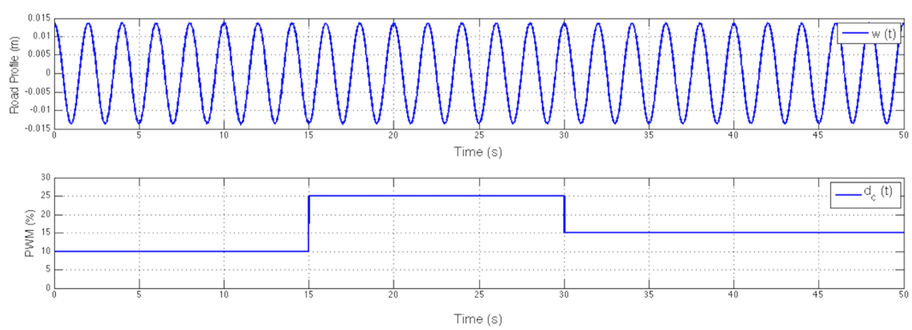

Figure 8: Simulation Scenario: *PWM* signal and Road Profile Disturbance

As explained by Tudón-Martínez, Fergani, Sename, Martinez, Morales-Menendez & Dugard (2015), some information about the dynamics of each road profile disturbance is assumed to be provided by a road identification scheme, prior to the proposed Fault Estimation structure. This information ($w_m(t)$) contains some part of $w(t)$, but some unknown disturbance ($\delta w(t)$) is still present. For the following simulation results, the known disturbance model $\mathbf{A}_{mw}$ (refer to Equation (11)) is different from the real disturbance's dynamic behaviour, in average of 15 % (plus some additive noise). This induces a modelling error that should be overlapped by the robustness of the mixed H_2/H_∞ extended observer approach.

Note that on a real test-bench, the variation of the loss of effectiveness faults α **are not** instantaneous, due to internal dynamics of the damper and other instrumentation contraints. These faults are better represented by slower ramps or first-order responses.

The following simulation case represents a trustworthy representation of an oil leakage fault, considering that a fault occurs at $t = 25\,\mathrm{s}$, when $\alpha(t)$ slowly starts to decrease to 0.5, finally stabilizing at $t = 55\,\mathrm{s}$. This is more realistic and closer to what will be presented as experimental results.

In Figure 9, one sees the expected (fault-less) damper force $F_{ER}(t)$ compared to the faulty $u_f(t) = \alpha(t)F_{ER}(t)$, according to the measured outputs $y(t)$, see Equation (4). These measured outputs $y(t)$ ($z_{def}(t)$ and $\ddot{z}_s(t)$) and the (numerically computed) deflection velocity $\dot{z}_{def}(t)$ are given in Figure 10.

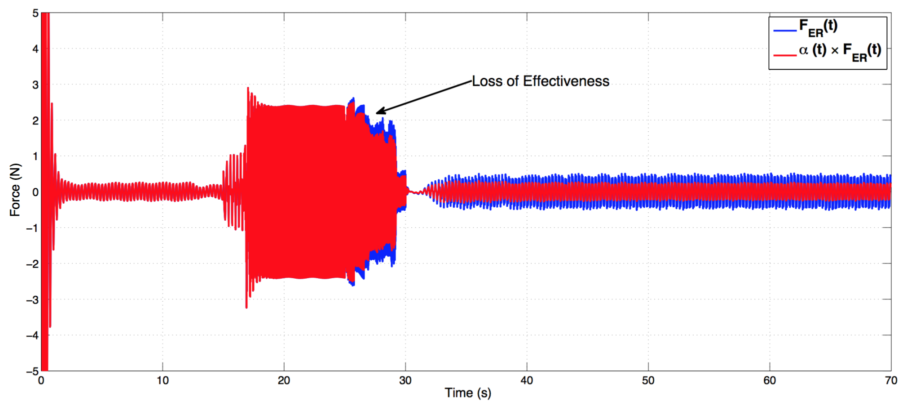

Figure 9: Faulty and Fault-Free (ideal) *ER* Damper Force

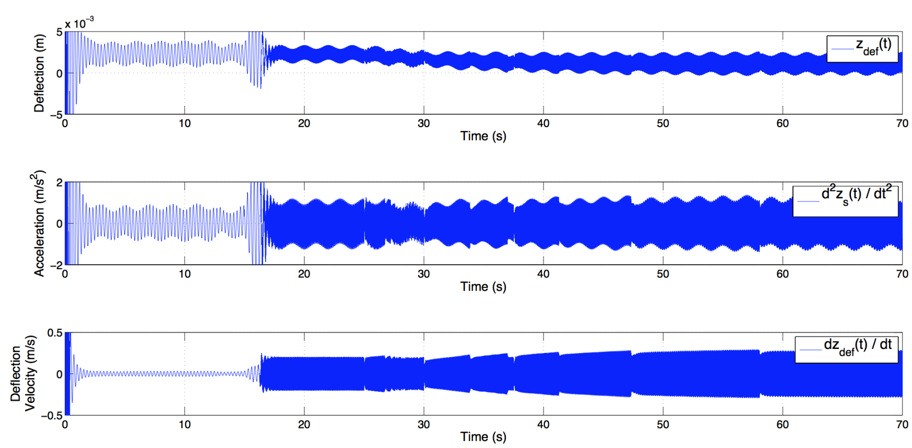

Figure 10: Measured Outputs and Deflection Velocity

Finally, the estimation of $\hat{\alpha}(t)$ by the proposed scheme is presented in Figure 11, compared to the actual value of the fault term $\alpha(t)$. Once again, one can observe a very accurate result in terms of simulation.

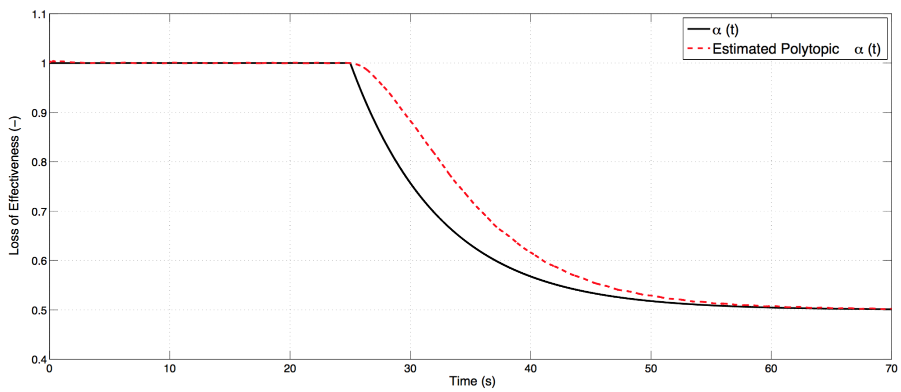

Figure 11: Simulation of Fault Estimation

Remark 6. In terms of comparisons, (Nguyen, Sename & Dugard, 2016) has already discussed that *LPV* observer-based *FE* schemes for suspension dampers present better results than the *FAFE* method or even parametric adaptive observers. Still, readers are invited to refer to Appendix Appendix A, wherein a simulation example is given comparing the proposed approach with a well-known sliding-mode technique.

5.2. Experimental Validation

Now, in order to thoroughly validate the approach for damper fault identification, some experimental tests on the vehicle testbed are presented. This is of most importance as it is a proof of the efficiency, reliability and feasibility of the proposed fault detection method.

The scenario considers a full vehicle running at 120 km/h in a straight line on a dry road, with a sequence of sinusoidal bumps (20 mm peak to peak). Figure 12 shows this road profile on the front-left corner of the vehicle. The information on this disturbance model $\mathbf{A}_{mw}$ is somewhat accurate, although there exist some modelling errors (δw) and noise because the real road profile is slightly different from the desired one due to the inner motor control system.

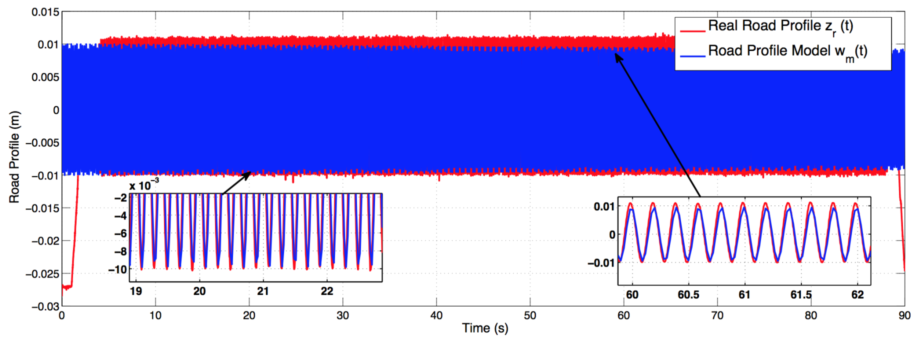

Figure 12: Experimental Validation Scenario: Road Profile

Remembering Figure 4, the damper is not controlled in closed-loop, but the PWM signal is used to mimic a fault on the physical ER damper. The signal $\overline{d_c}(t)$ is taken fixed at 30 %, whereas the actual signal sent to the damper, $d_c(t)$, varies in order to mimic a desired fault.

For the explained validation goals, a fault is mimicked at $t = 45$ s as a single decreasing step from $\alpha = 1$ to $\alpha = 0.5$. This could represent an oil leakage or even the effect of extremely high temperatures upon the damper. Figure 13 shows the expected (faultless) damper force compared with the real (faulty) damper fault. The expected damper force $u(t) = F_{ER}(t)$ is computed with the use of equations (12)-(16) taking a constant PWM signal at 30 %, whereas the actual damper force comes from a force sensor present on the used vehicle test-bench (see Figure 2). As it can be seen, the effect of the mimicked fault is not instantaneous, and there is a decreasing dynamic before α stabilizes.

The measured system outputs for this validation scenario are seen in Figure 14. Real measurements are $z_{def}(t)$ and $\ddot{z}_s(t)$, whereas $\dot{z}_{def}(t)$ is computed numerically. Obviously, these measurements are corrupted by some noises - always present due to (physical) instrumentation.

Finally and most importantly, in Figure 15, the detection of the fault factor α is presented and compared with the (virtually set) real value. This proves the worthiness of the LPV FE approach proposed in this paper and shows how it can be efficiently used for the identification of faults on real ER dampers of automotive suspension systems. The accuracy on experimental validation is, obviously, not as strong as on simulation, due to physical instrumentation constraints, nonlinearities and noise. Nonetheless, the approach is **strong** to detect faults on dampers.

5.3. Overall Analysis

As showed by simulation results and experimental validation, the proposed fault detection approach is able to efficiently estimate faults on ER dampers of vehicular semi-active suspension systems. The proposed approach is accurate

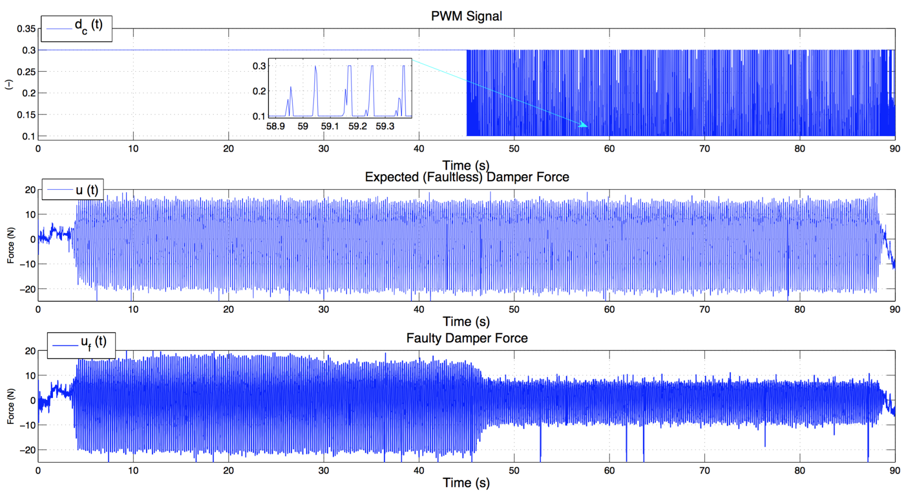

Figure 13: Experimental Validation Scenario: *PWM* Signal

and the mixed H_2/H_∞ (noise-filtering and disturbance attenuation) extended observer formulation is able to efficiently reduce the noise effect and disturbances on the estimation of each fault α.

It has to be remarked, still, that the industrial *state-of-practice* of fault estimation/detection applied to *ER* dampers is null, inexistent. Thus, as the method proposed herein is simple and easy to implement, it could well be used in the near future by industrial damper manufacturers.

6. Conclusion

This paper presented the issue of fault estimation for Electro-Rheological dampers of semi-active Automotive Suspension systems, considering a polytopic *LPV*-based strategy. As evidenced different results, including experimental validation, the proposed scheme is able to collect efficient, accurate and timely information on the possible damper faults, by solely considering the use of a *Quarter of Vehicle* model, a parametric dynamic damper model and a mixed H_2/H_∞ *LPV* observer synthesis, without the need for any additional sensors or physical components.

Such *FE* scheme could be used for fault tolerant control purposes of suspensions systems in the presence of damper faults, in order to preserve the system stability or some performance specifications, despite the presence of faults.

For future works, the authors plan on analyzing and surveying other possible *LPV*-based fault detection techniques that can be implemented without new components and can be verified experimentally.

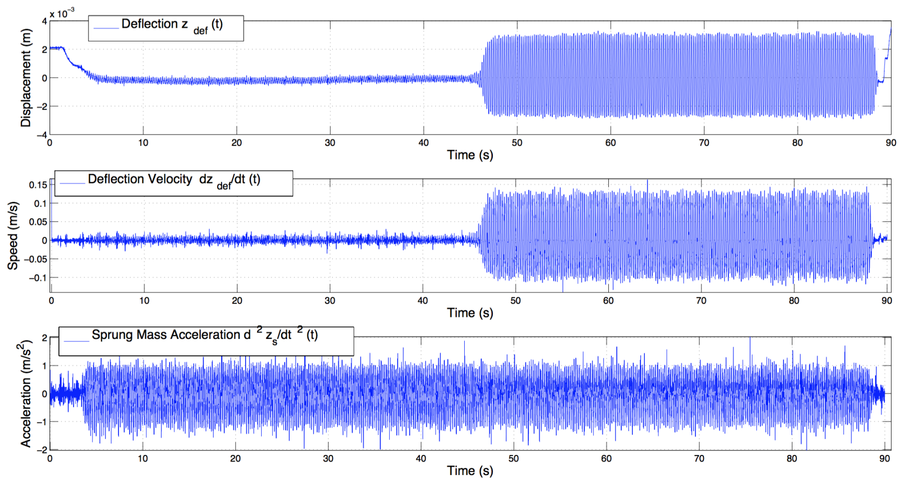

Figure 14: Experimental Validation Scenario: Measured Outputs

Acknowledgements

This work has been partially supported by the *LabEx PERSYVAL-Lab* ($ANR-11-LABX-0025-01$), funded by the French program *Investissements d'avenir*. The authors also thank *CAPES* for financing project *BRAFITEC ECoSud*.

References

Alwi, H., Edwards, C., & Marcos, A. (2012). Fault reconstruction using a LPV sliding mode observer for a class of LPV systems. *Journal of the Franklin Institute*, *349*, 510–530.

Blanke, M., Izadi-Zamanabadi, R., Bogh, S., & Lunau, C. (1997). Fault-tolerant control systems - a holistic view, .

Blanke, M., Staroswiecki, M., & Wu, N. E. (2001). Concepts and methods in fault-tolerant control. In *American Control Conference, 2001. Proceedings of the 2001* (pp. 2606–2620). IEEE volume 4.

Chen, J., & Patton, R. J. (2012). *Robust model-based fault diagnosis for dynamic systems* volume 3. Springer Science & Business Media.

Chen, L., Patton, R., & Goupil, P. (2016a). Application of model-based LPV actuator fault estimation for an industrial benchmark. *Control Engineering Practice*, *56*, 60–74.

Chen, L., Patton, R., & Goupil, P. (2016b). Robust fault estimation using an LPV reference model: ADDSAFE benchmark case study. *Control Engineering Practice*, *49*, 194–203.

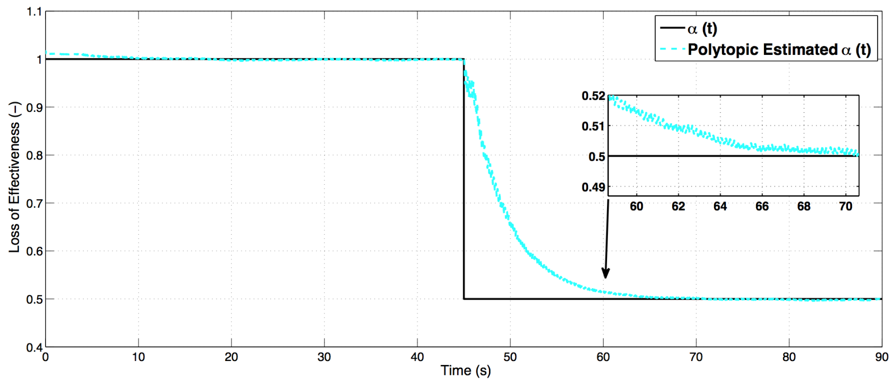

Figure 15: Experimental Validation: *ER* Damper Fault Estimation

De Persis, C., & Isidori, A. (2001). A geometric approach to nonlinear fault detection and isolation. *IEEE transactions on automatic control*, *46*, 853–865.

Do, A.-L., Sename, O., & Dugard, L. (2010). An LPV control approach for semi-active suspension control with actuator constraints. In *American Control Conference (ACC), 2010* (pp. 4653–4658). IEEE.

Doumiati, M., Martinez, J., Sename, O., Dugard, L., & Lechner, D. (2017). Road profile estimation using an adaptive youla–kučera parametric observer: Comparison to real profilers. *Control Engineering Practice*, *61*, 270–278.

Ducard, G., & Geering, H. P. (2008). Efficient nonlinear actuator fault detection and isolation system for unmanned aerial vehicles. *Journal of Guidance, Control, and Dynamics*, *31*, 225–237.

Edwards, C., Spurgeon, S. K., & Patton, R. J. (2000). Sliding mode observers for fault detection and isolation. *Automatica*, *36*, 541–553.

Fergani, S., Menhour, L., Sename, O., Dugard, L., & D'Andréa-Novel, B. (2016). Integrated vehicle control through the coordination of longitudinal/lateral and vertical dynamics controllers: Flatness and LPV/h_∞-based design. *International Journal of Robust and Nonlinear Control*, .

Fergani, S., Menhour, L., Sename, O., Dugard, L., & Novel, B. (2014a). Full vehicle dynamics control based on LPV/hinf and flatness approaches. In *Control Conference (ECC), 2014 European* (pp. 2346–2351). IEEE.

Fergani, S., Sename, O., & Dugard, L. (2014b). A LPV/h_∞ fault tolerant control of vehicle roll dynamics under semi-active damper malfunction. In *American Control Conference (ACC), 2014* (pp. 4482–4487). IEEE.

Fischer, D., & Isermann, R. (2004). Mechatronic semi-active and active vehicle suspensions. *Control engineering practice*, *12*, 1353–1367.

Gao, Z., & Ding, S. X. (2007). Actuator fault robust estimation and fault-tolerant control for a class of nonlinear descriptor systems. *Automatica*, *43*, 912–920.

Gertler, J. (1997). Fault detection and isolation using parity relations. *Control engineering practice*, *5*, 653–661.

Grenaille, S., Henry, D., & Zolghadri, A. (2008). A method for designing fault diagnosis filters for LPV polytopic systems. *Journal of Control Science and Engineering*, *2008*, 1.

Guo, L.-X., & Zhang, L.-P. (2012). Robust h_∞ control of active vehicle suspension under non-stationary running. *Journal of Sound and Vibration*, *331*, 5824–5837.

Guo, S., Yang, S., & Pan, C. (2006). Dynamic modeling of magnetorheological damper behaviors. *Journal of Intelligent material systems and structures*, *17*, 3–14.

Hamayun, M. T., Edwards, C., & Alwi, H. (2016). Design and analysis of an integral sliding mode fault tolerant control scheme. In *Fault Tolerant Control Schemes Using Integral Sliding Modes* (pp. 39–61). Springer.

Henry, D., & Zolghadri, A. (2005). Design of fault diagnosis filters: A multi-objective approach. *Journal of the Franklin Institute*, *342*, 421–446.

Hernández-Alcántara, D., Tudón-Martínez, J. C., Amézquita-Brooks, L., Vivas-López, C. A., & Morales-Menéndez, R. (2016). Modeling, diagnosis and estimation of actuator faults in vehicle suspensions. *Control Engineering Practice*, *49*, 173–186.

Hrovat, D. (1997). Survey of advanced suspension developments and related optimal control applications. *Automatica*, *33*, 1781–1817.

Hrovat, D., & Hubbard, M. (1987). A comparison between jerk optimal and acceleration optimal vibration isolation. *Journal of Sound and Vibration*, *112*, 201–210.

Isermann, R. (1997). Supervision, fault-detection and fault-diagnosis methodsan introduction. *Control engineering practice*, *5*, 639–652.

ISO 8608:2016 (2016). *Measurement and Evaluation of mechanical vibration and shock as applied to machines, vehicles and structures*. Standard International Organization for Standardization.

Jiang, J., & Yu, X. (2012). Fault-tolerant control systems: A comparative study between active and passive approaches. *Annual Reviews in control*, *36*, 60–72.

Karimi, H. R. (2008). Observer-based mixed h2/h control design for linear systems with time-varying delays: An lmi approach. *International Journal of Control, Automation and Systems*, *6*, 1–14.

Khosrowjerdi, M. J., Nikoukhah, R., & Safari-Shad, N. (2004). A mixed h2/h approach to simultaneous fault detection and control. *Automatica*, *40*, 261–267.

Kulcsár, B., & Verhaegen, M. (2012). Robust inversion based fault estimation for discrete-time LPV systems. *IEEE Transactions on Automatic Control*, *57*, 1581–1586.

Lofberg, J. (2004). *yalmip*: A toolbox for modeling and optimization in matlab. *IEEE International Symposium on Computer Aided Control Systems Design*, (pp. 284–289). doi:10.1109/CACSD.2004.1393890.

López-Estrada, F.-R., Ponsart, J.-C., Astorga-Zaragoza, C., & Theilliol, D. (2013). Fault estimation observer design for descriptor-LPV systems with unmeasurable gain scheduling functions. In *Conference on Control and Fault-Tolerant Systems* (pp. 269–274). IEEE.

Mahmoud, M., Jiang, J., & Zhang, Y. (2003). *Active fault tolerant control systems: stochastic analysis and synthesis* volume 287. Springer Science & Business Media.

Mathworks (2017). MATLAB *r*2017*a*.

Mohammadpour, J., & Scherer, C. W. (2012). *Control of linear parameter varying systems with applications*. Springer Science & Business Media.

Moradi, M., & Fekih, A. (2014). Adaptive PID-sliding-mode fault-tolerant control approach for vehicle suspension systems subject to actuator faults. *IEEE Transactions on Vehicular Technology*, *63*, 1041–1054.

Nguyen, M. Q., Sename, O., & Dugard, L. (2015). A switched LPV observer for actuator fault estimation. *IFAC-PapersOnLine*, *48*, 194–199.

Nguyen, M. Q., Sename, O., & Dugard, L. (2016). Comparison of observer approaches for actuator fault estimation in semi-active suspension systems. In *3rd Conference on Control and Fault-Tolerant Systems* (pp. 227–232). IEEE.

Nguyen, Q.-H., & Choi, S.-B. (2009). A new approach for dynamic modeling of an electrorheological damper using a lumped parameter method. *Smart Materials and Structures*, *18*, 115020.

de Oca, S., Puig, V., Witczak, M., & Dziekan, Ł. (2012). Fault-tolerant control strategy for actuator faults using LPV techniques: Application to a two degree of freedom helicopter. *International Journal of Applied Mathematics and Computer Science*, *22*, 161–171.

Pardalos, P. M., Migdalas, A., & Pitsoulis, L. (2008). *Pareto optimality, game theory and equilibria* volume 17. Springer Science & Business Media.

Patten, W., He, Q., Kuo, C., Liu, L., & Sack, R. (1994). Suppression of vehicle induced bridge vibration via hydraulic semi-active vibration dampers. In *Proceeding of the 1st world conference on structural control* (pp. 30–38). volume 3.

Poussot-Vassal, C. (2008). *Robust LPV multivariable Automotive Global Chassis Control*. Ph.D. thesis Institut National Polytechnique de Grenoble-INPG.

Poussot-Vassal, C., Sename, O., Dugard, L., Gaspar, P., Szabo, Z., & Bokor, J. (2011). Attitude and handling improvements through gain-scheduled suspensions and brakes control. *Control Engineering Practice*, *19*, 252–263.

Poussot-Vassal, C., Spelta, C., Sename, O., Savaresi, S. M., & Dugard, L. (2012). Survey and performance evaluation on some automotive semi-active suspension control methods: A comparative study on a single-corner model. *Annual Reviews in Control*, *36*, 148–160.

Rodrigues, M., Hamdi, H., Theilliol, D., Mechmeche, C., & BenHadj Braiek, N. (2015). Actuator fault estimation based adaptive polytopic observer for a class of LPV descriptor systems. *International Journal of Robust and Nonlinear Control*, *25*, 673–688.

Rotondo, D., López-Estrada, F.-R., Nejjari, F., Ponsart, J.-C., Theilliol, D., & Puig, V. (2016). Actuator multiplicative fault estimation in discrete-time LPV systems using switched observers. *Journal of the Franklin Institute*, *353*, 3176–3191.

Sammier, D., Sename, O., & Dugard, L. (2003). Skyhook and h_∞ control of semi-active suspensions: some practical aspects. *Vehicle System Dynamics*, *39*, 279–308.

Savaresi, S. M., Bittanti, S., & Montiglio, M. (2005). Identification of semi-physical and black-box non-linear models: the case of MR-dampers for vehicles control. *Automatica*, *41*, 113–127.

Savaresi, S. M., Poussot-Vassal, C., Spelta, C., Sename, O., & Dugard, L. (2010). *Semi-active suspension control design for vehicles*. Elsevier.

Scherer, C., Gahinet, P., & Chilali, M. (1997). Multiobjective output-feedback control via lmi optimization. *IEEE Transactions on automatic control*, *42*, 896–911.

Sename, O., Tudón-Martínez, J. C., & Fergani, S. (2013). LPV methods for fault-tolerant vehicle dynamic control. In *Conference on Control and Fault-Tolerant Systems* (pp. 116–130). doi:10.1109/SysTol.2013.6693821.

Toh, K.-C., Todd, M. J., & Tütüncü, R. H. (1999). Sdpt3a matlab software package for semidefinite programming, version 1.3. *Optimization methods and software*, *11*, 545–581.

Tseng, H. E., & Hrovat, D. (2015). State of the art survey: active and semi-active suspension control. *Vehicle system dynamics*, *53*, 1034–1062.

Tudón-Martínez, J. C., Fergani, S., Sename, O., Martinez, J. J., Morales-Menendez, R., & Dugard, L. (2015). Adaptive road profile estimation in semiactive car suspensions. *IEEE Transactions on Control Systems Technology*, *23*, 2293–2305.

Tudon-Martinez, J. C., Varrier, S., Sename, O., Morales-Menendez, R., Martinez, J.-J., & Dugard, L. (2013). Fault tolerant strategy for semi-active suspensions with LPV accommodation? In *Control and Fault-Tolerant Systems (SysTol), 2013 Conference on* (pp. 631–636). IEEE.

Tudón-Martínez, J. C., Varrier, S., Sename, O., Morales-Menendez, R., Martinez, J. J., & Dugard, L. (2013). Fault tolerant strategy for semi-active suspensions with LPV accommodation? In *Conference on Control and Fault-Tolerant Systems* (pp. 631–636). doi:10.1109/SysTol.2013.6693942.

Unger, A., Schimmack, F., Lohmann, B., & Schwarz, R. (2013). Application of LQ-based semi-active suspension control in a vehicle. *Control Engineering Practice*, *21*, 1841–1850.

Vivas-Lopez, C., Alcántara, D. H., Nguyen, M. Q., Fergani, S., Buche, G., Sename, O., Dugard, L., & Morales-Menéndez, R. (2010). INOVE: Integrated approach for observation and control of vehicle dynamics. http://www.gipsa-lab.fr/projet/inove/index.html. Accessed: 13/10/2016.

Vivas-Lopez, C., Alcántara, D. H., Nguyen, M. Q., Fergani, S., Buche, G., Sename, O., Dugard, L., & Morales-Menéndez, R. (2014). INOVE: a test-bench for the analysis and control of automotive vertical dynamics. In *14th International Conference on Vehicle System Dynamics, Identification and Anomalies (VSDIA 2014)*.

Wang, H., Chen, H., & Weng, Z. (2014). Fault estimation for LPV system with LFT parameter dependence. In *IEEE International Conference on Information and Automation* (pp. 560–565). IEEE.

Xiao, B., Hu, Q., & Zhang, Y. (2012). Adaptive sliding mode fault tolerant attitude tracking control for flexible spacecraft under actuator saturation. *IEEE Transactions on Control Systems Technology*, *20*, 1605–1612.

Yamamoto, K., Koenig, D., Sename, O., & Moulaire, P. (2015). Driver torque estimation in electric power steering system using an h_∞/h_2 proportional integral observer. In *Decision and Control (CDC), 2015 IEEE 54th Annual Conference on* (pp. 843–848). IEEE.

Zhang, K., Jiang, B., & Chen, W. (2009a). An improved adaptive fault estimation design for polytopic LPV systems with application to helicopter models. In *Asian Control Conference, 2009. ASCC 2009. 7th* (pp. 1108–1113). IEEE.

Zhang, K., Jiang, B., & Cocquempot, V. (2009b). Fast adaptive fault estimation and accommodation for nonlinear time-varying delay systems. *Asian Journal of Control*, *11*, 643–652.

Zhang, K., Jiang, B., & Shi, P. (2012). *Observer-based fault estimation and accomodation for dynamic systems* volume 436. Springer.

Zhang, Y., & Jiang, J. (2008). Bibliographical review on reconfigurable fault-tolerant control systems. *Annual reviews in control*, *32*, 229–252.

Appendix A. Simulation Comparison

In this Section, the proposed *polytopic LPV FE* scheme is compared to a Sliding-Mode fault reconstruction approach, as proposed by Alwi, Edwards & Marcos (2012). This is once again done with a realistic, nonlinear vehicle model. For this, a simple single-step scenario is taken, wherein the loss of effectiveness fault $\alpha(t)$ decreases at $t = 25$ s to 0.85.

Once again, the same road profile $w(t)$ and PWM signal $d_c(t)$ seen in Figure 8 are used. Figure A.16 shows the expected (fault-less) damper force $F_{ER}(t)$ compared to the faulty $u_f(t) = \alpha(t)F_{ER}(t)$, according to the measured outputs $y(t)$. These measured outputs $y(t)$ and the (numerically computed) deflection velocity $z_{def}(t)$ are seen in Figure A.17.

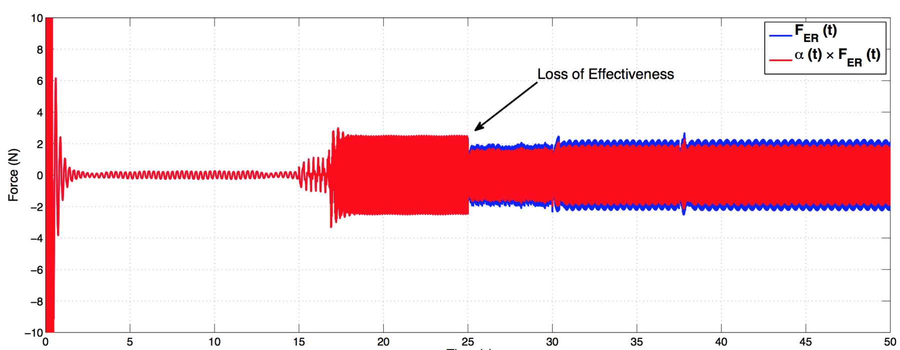

Figure A.16: Simulation Comparison: Faulty and Fault-Free (ideal) *ER* Damper Force

The estimation of $\hat{\alpha}(t)$ by both approaches is given in Figure A.18, and compared to the actual value of $\alpha(t)$.

Compared with the very common *sliding-mode* fault reconstruction approach, discussed in (Edwards, Spurgeon & Patton, 2000; Xiao, Hu & Zhang, 2012;

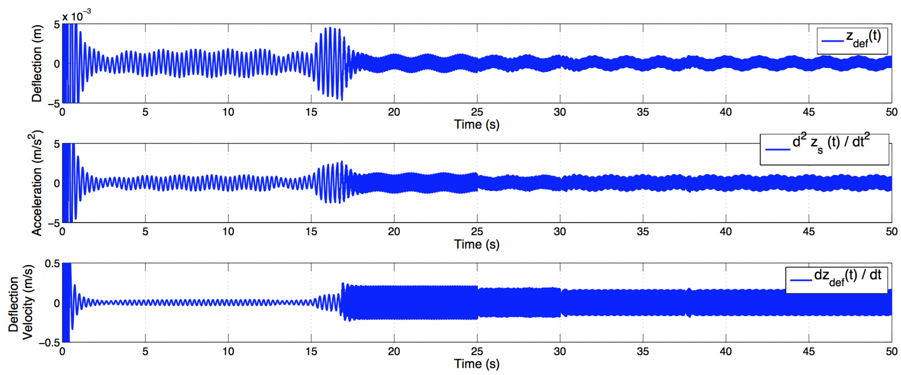

Figure A.17: Simulation Comparison: Measured Outputs and Deflection Velocity

Hamayun, Edwards & Alwi, 2016), the proposed *Polytopic LPV* scheme yields more efficient and accurate results. Even though the sliding-mode approach is fast, it does not conclude on how much loss does the damper present. An accurate fault estimation scheme can be used for Fault Tolerance goals, to reconfigure the control law in such way that driving performances of the vehicle are maintained. With the sliding-mode approach, this would not be possible, but with the proposed approach, direct.

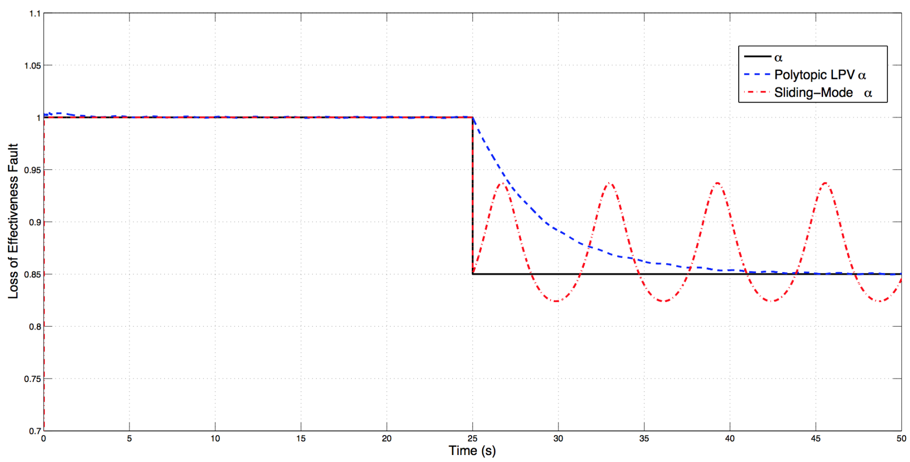

Figure A.18: Simulation of Fault Estimation Comparison to *Sliding-Mode* Approach